HHS Public Access

Author manuscript

Adv Mater. Author manuscript; available in PMC 2016 April 01.

Published in final edited form as:

Adv Mater. 2015 April ; 27(13): 2216–2223. doi:10.1002/adma.201405337.

In situ forming growth factor-loaded coacervate microparticle-embedded hydrogel for directing encapsulated stem cell fate

Dr. Oju Jeon,
Department of Biomedical Engineering, Case Western Reserve University Cleveland, OH 44106, USA

David W. Wolfson, and
Department of Biomedical Engineering, Case Western Reserve University Cleveland, OH 44106, USA

Prof. Eben Alsberg
Department of Biomedical Engineering, Case Western Reserve University Cleveland, OH 44106, USA. Department of Orthopaedic Surgery, Case Western Reserve University Cleveland, OH 44106, USA

Eben Alsberg: eben.alsberg@case.edu

Keywords

microencapsulation; coacervate; alginate; gelatin; microdroplet

Complex coacervation is liquid-liquid phase separation in an aqueous solution by spontaneous aggregation associated with electrostatic matching between two oppositely charged polyelectrolytes.[1,2] Despite their potential in medical and food applications, complex coacervates had not been heavily researched since the introduction of the term in 1929 by Bungenberg de Jong and Kruyt[3] until only the past decade when interest in the area increased dramatically in relation to new engineered biological systems.[4] Complex coacervates have been used for direct complexation between bioactive molecules and polysaccharides,[5,6] micro- or nanoencapsulation of bioactive molecules or cells,[7,8] and surface coating of particles,[9] due to their unique physicochemical characteristics that can be easily modulated by pH, ionic strength, charge density, and the stoichiometry of interacting molecules.[6,7,8,9] However, these systems often require cytotoxic surfactants and/or expensive equipment. The ability to cheaply form cytocompatible coacervates under mild conditions that permit the compartmentalized encapsulation of cells and bioactive factors via simple mixing would be valuable for tissue engineering strategies, as it would allow for control over their spatial distribution.[10] This spatial control over the location of cells and bioactive factors may better facilitate the regional regulation of encapsulated cell fate, which is critical for the engineering of complex tissues. However, to the best of our knowledge, no coacervate system has been reported capable of simultaneous cell

Correspondence to: Eben Alsberg, eben.alsberg@case.edu.

Supporting Information

Supporting Information is available from the Wiley Online Library or from the author.

encapsulation and the formation of drug-laden microdroplets under cytocompatible conditions that could be used as a three-dimensional biomaterial for cell encapsulation and transplantation, and tissue engineering applications, due to the harsh physicochemical conditions [i.e., low pH (< 4) and high temperature (~ 60 °C)] typically required for complex coacervation formation.[11,12]

One well-known example of complex coacervation that has been widely studied in colloid science is the sodium alginate-gelatin coacervate system.[11,12,13] The biocompatible polymer pair interacts to form a complex coacervate under low pH conditions and polymer concentrations. Herein, we describe the spontaneous formation and properties of coacervates and/or coacervate-laden photocrosslinked hydrogels derived from the simple mixing of OMA and GelMA in aqueous solution at a wide pH range and room temperature, and demonstrate that the resultant compartments can be utilized as novel platforms for localized, sustained bioactive molecule delivery systems with the capacity for the simultaneous encapsulation of stem cells, such as mesenchymal stem cells (MSCs), for therapeutic applications like bone tissue engineering.

OMA was prepared by functionalization of alginate by both oxidation and methacrylation (Figure 1a),[14] and GelMA was synthesized by methacrylating gelatin (Figure 1b).[15] By mixing aqueous solutions of OMA and GelMA, imine bond-based complex coacervate microdroplets can form via Schiff base reaction between the aldehyde groups of the OMA and the amine groups of the GelMA (Figure 1c). In this manner, micron-scale coacervates (Figure 1d–f, Figure S3a–b and Supplementary Movie S1) and coacervate-laden hydrogels formed by photocrosslinking immediately after mixing (Figure S3c) were easily generated. The morphological changes in the OMA/GelMA coacervates resulting from varying the degrees of alginate oxidation and methacrylation were first investigated. When varying the theoretical methacrylation level of OMA (15, 25 and 45%) while keeping a constant theoretical oxidation level of 10 % (10OX15MA, 10OX25MA, and 10OX45MA), after mixing with highly methacrylated type-A gelatin (H-GelMA-A) and type-B gelatin (H-GelMA-B) solutions, coacervate microdroplets formed that were not uniformly spherical in structure. In contrast, solutions of H-GelMA mixed with OMAs of 17.5 % and 25 % theoretical oxidation exhibited relatively homogeneous spherical complex coacervate microdroplets (Figure S3a–b). Since the crosslinking by imine bond-based complexation between OMA and H-GelMA depends on the number of aldehyde groups of OMA, and 17.5OX and 25OX OMA had 1.57 and 2.23-fold higher aldehyde groups than 10OX OMAs (Supplementary Table S1), respectively, it is likely that the OMA/H-GelMA coacervate microdroplets have higher crosslinking density with increasing alginate oxidation level, which could enhance the physical stability of coacervate microdroplets.

Since turbidity is one of most important indicators to confirming coacervation,[16] we evaluated turbidity before and after mixing of the two solutions by absorbance measurement at 500 nm to determine the degrees of complex coacervate formation. Regardless of gelatin type and alginate oxidation and methacrylation level, the turbidity of all conditions significantly increased after mixing, indicating complex coacervate formation (Figure 1g). As the alginate oxidation level increased, the turbidity of the OMA/H-GelMA complex coacervates also exhibited an increasing trend, indicating more stable coacervate formation.

This result was well correlated with microscopic examination of the morphology of the coacervates. However, as the alginate methacrylation level increased, which could decrease the number of negatively charged carboxylic acid groups in alginate, the turbidity of the OMA/H-GelMA coacervates showed a decreasing trend. This result indicates that the electrostatic interactions of carboxylic acid groups of OMA and amine groups of H-GelMA could also affect the coacervate formation of OMA and H-GelMA.

The phase separation in typical complex coacervation is primarily caused by the electrostatic interactions between oppositely charged polyelectrolytes such as proteins and polymers.[2] Therefore, pH, which influences the ionic strength of polyelectrolytes, plays a fundamental role in the formation of complexes between oppositely charged polyelectrolytes.[9] Since the capacity for complex coacervate formation by the alginate/gelatin system has exhibited a strong dependence on pH in previous reports,[11] the turbidity of OMA/GelMA coacervates at various pHs (2.07 ~ 11.57) was measured to determine if there was a similar pH dependency for these functionalized polymers. Interestingly, the mixtures of OMA and H-GelMA formed coacervates at a wide range of pH, demonstrating a pH independency, with higher turbidity observed at lower pH (Figure 1h). This result indicates that the complex coacervates were mainly formed through imine bond formation by Schiff base reaction, which takes place at a wide range of pHs,[17] between the aldehyde groups of OMA and the amine groups of H-GelMA as shown in Figure 1c, while the electrostatic interactions between the carboxylic groups of OMA and the amine groups of H-GelMA had greater affect on the complex coacervate formation at lower pH, which is in agreement with the literature.[11]

Since the spatial distribution of polymers can significantly influence the properties of complex coacervate systems,[8,18] OMA and GelMA were modified with water-soluble blue fluorescent CF^{TM}-350 and red fluorescent CF^{TM}-633 dyes, respectively (Figure 2a and b) to visualize the distribution of the polymers in this coacervate system. As shown in Figure 2c–e, coacervate microdroplets were primarily composed of H-GelMA-A (red), while OMA (blue) was mainly observed in the surrounding equilibrium phase. Furthermore, high-magnification images of an individual coacervate microdroplet showed that H-GelMA-A was uniformly distributed throughout the coacervate microdroplet (Figure 2f and h), while OMA was observed on the surface shell of coacervate microdroplet (Figure 2g and h). Figure 2i schematically illustrates the proposed mechanism of OMA/GelMA coacervate formation and resulting microstructure. Upon mixing the two solutions (Figure 2i–1), the GelMA can form imine bond-based covalent complexes with OMA (Figure 2i–2) regardless of GelMA and OMA's ionic charge. Since methacrylate groups are hydrophobic, methacrylation of alginate and gelatin could increase their hydrophobicity. Because gelatin tends to aggregate by hydrophobic interactions,[19] which is further enhanced by its methacrylation, GelMA can more rapidly aggregate and form coacervate droplets within a few seconds (Movie S1). Finally, OMA/GelMA complexes were located on the surface of coacervate microdroplets and formed an outer boundary (Figure 2g and 2i–3), which could stabilize OMA/GelMA coacervate microdroplets after mixing the solutions.

To further support our proposed mechanism for OMA/GelMA coacervation, which is induced by the crosslinking by imine bond formation between OMA and GelMA, and

examine a potential key role of the methacrylate groups of GelMA in coacervate formation, we evaluated coacervate formation using oxidized alginate (OA), OMA, Gelatin-A and GelMA-A. The mixtures of OA/Gelatin-A (Figure 3a), OMA/Gelatin-A (Figure 3b), and OA/Gelatin-A with low level of methacrylation (L-GelMA-A) (Figure 3c) did not form coacervates, but instead formed chemically crosslinked and transparent hydrogels. In contrast, mixtures of OA/Gelatin-A with high level of methacrylation (H-GelMA-A) (Figure 3d), OMA/L-GelMA-A (Figure 3e), and OMA/H-GelMA-A (Figure 3f) formed coacervate microdroplets. These results were further confirmed by turbidity measurements of the mixtures (Figure S4a–e).

Based on these results, we proposed the structure of each system and confirmed it through fluorescence microscopy. In the OA and Gelatin-A mixture without any methacrylate groups, macromers and water molecules were homogenously distributed in the imine bond-crosslinked hydrogels (Figure 3g). OMA/Gelatin-A (Figure 3h) and OA/L-GelMA-A (Figure 3i) mixtures were also crosslinked by imine bond formation, but hydrophobic interactions by crosslinking and methacrylation were insufficient to induce phase separation due to the low concentration of methacrylates. Therefore, they also formed crosslinked transparent hydrogels. This was not the case for OA/H-GelMA-A (Figure 3j), OMA/L-GelMA-A (Figure 3k) and OMA/H-GelMA-A (Figure 3l) mixtures, however, which had sufficient number of hydrophobic domains that consisted of chemical crosslinking and methacrylate groups, and in turn induced liquid-liquid phase separation to form coacervates. The fluorescence photomicrographs provide microstructural data that supports the proposed mechanism for coacervate formation in this system.

Since solutions of OA with L-GelMA-A did not form a complex coacervate but H-GelMA-A did, this indicates that methacrylate concentration in the gelatin solution plays an important role in the process. To elucidate the relationship between coacervate formation and gelatin methacrylation level, turbidity measurements were taken of mixtures of OA solution with gelatin solutions containing various weight fractions of H-GelMA-A. The turbidity of the mixture gradually increased as the H-GelMA-A content increased up to 10 % in gelatin solution, and then rapidly increased at > 10 % H-GelMA-A in the gelatin solution (Figure S4f). This result clearly demonstrates the dependence of OMA/GelMA coacervate formation on the concentration of hydrophobic methacrylate groups in the gelatin solution.

This OMA/GelMA coacervation systems exhibit microdroplet formation in OMA equilibrium phase, which can be further photocrosslinked in the presence of low level UV light and a photoinitiator to form a hydrogel. Microspheres containing bioactive molecules can be easily incorporated and homogenously distributed within the hydrogel through this coacervation approach for localized delivery and exposure of these molecules in a controlled and sustained manner over time to cells incorporated in the microspheres, in the equilibrium phase of the hydrogel and/or surrounding the hydrogel (Figure 4a). To investigate whether incorporating human bone morphogenetic protein-2 (BMP-2) into the GelMA solution, which mainly comprised the resulting coacervate microdroplets, could delay the release of the growth factor, compared to BMP-2 in the OMA solution, the release profiles of BMP-2 from two different coacervate-laden hydrogel systems were measured (Figure 4b; see

Supplementary Information for more details). The growth factor release from OMA/GelMA coacervate hydrogels when BMP-2 was originally in the OMA solution (red triangles) was more rapid than release from coacervates formed with BMP-2 originally in the GelMA solution (black circles). The release of BMP-2 could be further delayed by the addition of photocrosslinkable heparin[20] into the coacervate hydrogels due to affinity binding between heparin and the growth factor (Figure S5). The affinity interactions result from electrostatic interactions between the negatively charged sulfate groups of heparin and the positively charged amino acid groups of the growth factor.

To investigate the effect of prolonged presentation of BMP-2 on the osteogenic differentiation of stem cells in this system, human mesenchymal stem cells (hMSCs) were photoencapsulated in OMA/GelMA coacervate hydrogels and cultured in osteogenic differentiation media. As shown in Figure 4c-e and Figure S6, high cell viability was observed throughout all groups for 4 weeks, indicating the mixing and photoencapsulation process, macromers, and the OMA/GelMA coacervate hydrogels themselves and their degradation products are cytocompatible. DNA content in the OMA/GelMA group without BMP-2 was higher compared to the BMP-2 delivery groups at days 14, 28, 42 and 56, while there was no significant difference between BMP-2 delivery groups (Figure S6b). Cell/hydrogel constructs were evaluated for hMSC osteogenic differentiation by measuring alkaline phosphatase (ALP) activity, which is an early osteogenic differentiation marker, determining relative mRNA expression of Runt-related transcription factor 2 (Runx2), which is one of the earlier and most specific osteogenic differentiation makers, and bone sialoprotein (BSP), which is a later osteogenic differentiation marker, staining for calcium using Alizarin red S, and quantifying calcium deposition. Compared to the OMA/GelMA group without BMP-2, the ALP activity of photoencapsulated hMSCs could more rapidly increase by BMP-2 delivery from the coacervate or equilibrium phase by day 28, and then gradually decreased (Figure 4f). When the BMP-2 was delivered from the coacervate phase, photoencapsulated hMSCs showed significantly higher ALP activity at day 28, compared to BMP-2 delivered form equilibrium phase, and maximal ALP activity over the duration of the experiment was quantified for both of these conditions at this time point. A quantitative analysis of mRNA expression levels of Runx2 and BSP were evaluated by real-time quantitative reverse transcription-polymerase chain reaction (qRT-PCR) (Figure 4g–h). Compared to the control group without BMP-2, hMSCs expressed significantly higher Runx2 by BMP-2 delivery from coacervate or equilibrium phase at day 14 (Figure 4g). In addition, Runx2 expression level of hMSCs in the OMA/BMP-2 in GelMA group was also significantly higher than that of the control group by day 28. Photoencapsulated hMSCs expressed significantly higher BSP when BMP-2 was delivered from the coacervate hydrogels compared to the controls at day 28, while there was no significant difference among any groups at day 14 (Figure 4h).

Since mineralization is the ultimate indicator of stem cell osteogenic differentiation,[21] the calcium deposition in the hMSC/hydrogel constructs was then visualized and quantified by Alizarin red staining and a calcium assay, respectively. Compared to the control group, more intense Alizarin red staining was observed in the BMP-2 delivery groups at days 28 and 56 (Figure 4i–j). Moreover, the intensity of the staining signal was greatest when the BMP-2 was loaded in the coacervate phase. As shown in Figure 4k, similar to the Alizarin red

staining results, calcium deposition was significantly higher up to day 112 in coacervate hydrogels groups delivering BMP-2 compared to the control group, with the highest calcium deposition in the OMA/BMP-2 in GelMA hydrogels likely due to BMP-2 presentation in the hydrogels for a longer period of time. As shown in Figure S7, heparin modification of coacervate hydrogels further enhanced the calcium deposition in the coacervate hydrogels. These results demonstrate that long-term presentation of bioactive BMP-2 in the coacervate hydrogels enhances osteogenic differentiation of photoencapsulated stem cells and bone-related mineralization of the extracellular environment.

Micro- or nanoparticle-incorporated hydrogels have been widely studied to achieve sustained localized delivery of bioactive molecules for tissue engineering applications such as regenerating bone or cartilage.[22] Localized and controlled spatial and temporal presentation of these bioactive molecule have been demonstrated to be valuable in regulating encapsulated cell behavior in such tissue engineering strategies.[23] However, In these systems, it can be technically challenging to fabricate the micro- or nanoparticles with encapsulated bioactive molecules without loss of their bioactivity due to use of organic solvents,[24] high temperatures[25] and/or shear stress.[25,26] In this study, a system has been successfully engineered for the spontaneous formation of coacervates and/or coacervate-laden photocrosslinked hydrogels derived from the simple mixing of OMA and GelMA in aqueous solutions at physiological conditions for long-term localized delivery of growth factor. We demonstrated that the resultant compartments could be utilized as a novel platform for localized, sustained bioactive molecule delivery to encapsulated stem cells for therapeutic applications like bone tissue engineering. In addition to delivery of a single growth factor, particle-based systems have also been implemented to present multiple growth factors, such as BMP-2 and BMP-7,[27] BMP-2 and insulin-like growth factor,[28] vascular endothelial growth factor (VEGF) and BMP-2,[29] and VEGF and platelet-derived growth factor (PDGF),[30] to drive and enhance biologic processes such as osteogenesis and angiogenesis. The coacervate system presented here exhibited differential release profiles of a single growth factor depending on whether heparin was used in the system and whether the growth factor was within the coacervate microdroplets or the surrounding equilibrium phase. Thus, the OMA/GelMA coacervate microdroplet-embedded hydrogel platform could be utilized for the regulated spatiotemporal presentation of multiple growth factors from the same system, which could synergistically enhance tissue regeneration.

In summary, the spontaneous formation of coacervate microdroplets and/or coacervate-laden photocrosslinked hydrogels derived from the simple mixing of photocrosslinkable OMA and GelMA over a wide pH range at room temperature has been demonstrated. This system enables simultaneous creation of drug-laden microdroplets and encapsulation of stem cells in photopolymerized coacervate hydrogels under physiological conditions and can be utilized as a novel platform for in situ formation of localized, sustained bioactive molecule delivery to encapsulated stem cells for therapeutic applications.

Experimental Section

Preparation of OMA/GelMA coacervates

All macromers were dissolved separately in Dulbecco's phosphate buffered saline (PBS, 20 w/v %) with a photoinitiator (2-Hydroxy-4′-(2-hydroxyethoxy)-2-methylpropiophenone, 0.05 w/v %, Sigma). GelMA solutions were added to the OMA solutions at an equal volume ratio, followed by mixing for 1 min, to produce the OMA/GelMA coacervate microdroplets The OMA/GelMA coacervate microdroplet solutions were spread on cover slips, and imaged using a fluorescence microscope (ECLIPSE TE 300, Nikon) equipped with a digital camera (Retiga-SRV, QImaging). Complete detailed methodology can be found in Supporting Information.

Supplementary Material

Refer to Web version on PubMed Central for supplementary material.

Acknowledgments

The authors thank Robyn Marks for research assistance. The authors gratefully acknowledge funding from the National Institutes of Health's National Institute of Arthritis And Musculoskeletal And Skin Diseases under award numbers R01AR063194 (EA), R21AR061265 (EA), and T32AR7505 (OJ), and the National Institute of Dental & Craniofacial Research under award number R56DE022376 (EA). The contents of this publication are solely the responsibility of the authors and do not necessarily represent the official views of the National Institutes of Health.

References

1. Piculell L, Lindman B. Adv Colloid Interface Sci. 1992; 41:149.Hunt JN, Feldman KE, Lynd NA, Deek J, Campos LM, Spruell JM, Hernandez BM, Kramer EJ, Hawker CJ. Adv Mater. 2011; 23:2327. [PubMed: 21491513]
2. Carlsson F, Linse P, Malmsten M. J Phys Chem B. 2001; 105:9040.
3. Bungenberg de Jong HG, Kruyt HR. Proc K Ned Akad, Wet. 1929; 32:849.
4. Schmitt C, Sanchez C, Desobry-Banon S, Hardy J. Crit Rev Food Sci. 1998; 38:689.de Kruif CG, Weinbreck F, de Vries R. Curr Opin Colloid In. 2004; 9:340.Schmitt C, Turgeon SL. Adv Colloid Interface Sci. 2011; 167:63. [PubMed: 21056401]
5. Chu HH, Gao J, Chen CW, Huard J, Wang YD. P Natl Acad Sci USA. 2011; 108:13444.Lee KW, Johnson NR, Gao J, Wang YD. Biomaterials. 2013; 34:9877. [PubMed: 24060423] Ball V, Winterhalter M, Schwinte P, Lavalle P, Voegel JC, Schaaf P. J Phys Chem B. 2002; 106:2357.
6. Chu H, Chen CW, Huard J, Wang Y. Biomaterials. 2013; 34:1747. [PubMed: 23211448]
7. Koga S, Williams DS, Perriman AW, Mann S. Nat Chem. 2011; 3:720. [PubMed: 21860462] Roy K, Mao HQ, Huang SK, Leong KW. Nat Med. 1999; 5:387. [PubMed: 10202926]
8. Kizilay E, Kayitmazer AB, Dubin PL. Adv Colloid Interfac. 2011; 167:24.
9. Hwang DS, Waite JH, Tirrell M. Biomaterials. 2010; 31:1080. [PubMed: 19892396]
10. Park H, Temenoff JS, Tabata Y, Caplan AI, Mikos AG. Biomaterials. 2007; 28:3217. [PubMed: 17445882]
11. Devi N, Hazarika D, Deka C, Kakati DK. J Macromol Sci A. 2012; 49:936.Shinde UA, Nagarsenker MS. Indian J Pharma Sci. 2009; 71:313.
12. Saravanan M, Rao KP. Carbohyd Polym. 2010; 80:808.
13. Arneodo C, Benoit JP, Thies C. Abstr Pap Am Chem S. 1987; 194:54.
14. Jeon O, Alt DS, Ahmed SM, Alsberg E. Biomaterials. 2012; 33:3503. [PubMed: 22336294] Jeon O, Samorezov JE, Alsberg E. Acta Biomater. 2014; 10:47. [PubMed: 24035886]

15. Nichol JW, Koshy ST, Bae H, Hwang CM, Yamanlar S, Khademhosseini A. Biomaterials. 2010; 31:5536. [PubMed: 20417964] Van Den Bulcke AI, Bogdanov B, De Rooze N, Schacht EH, Cornelissen M, Berghmans H. Biomacromolecules. 2000; 1:31. [PubMed: 11709840]
16. Priftis D, Tirrell M. Soft Matter. 2012; 8:9396.
17. Gorostidi GRE, Basagoitia A, Blanco JGS, Blanco FG. J Mol Catal a-Chem. 1998; 129:173.
18. Srivastava A, Waite JH, Stucky GD, Mikhailovsky A. Macromolecules. 2009; 42:2168. [PubMed: 20808713]
19. Xu J, Xu Z, Qiao CD, Li TD. Colloids and surfaces B, Biointerfaces. 2014; 114:310.
20. Jeon O, Powell C, Solorio LD, Krebs MD, Alsberg E. J Control Release. 2011; 154:258. [PubMed: 21745508]
21. Jeon O, Alsberg E. Adv Func Mater. 2013; 23:4765.
22. Jeon O, Song SJ, Yang HS, Bhang SH, Kang SW, Sung MA, Lee JH, Kim BS. Biochem Biophys Res Comm. 2008; 369:774. [PubMed: 18313401] Ding D, Zhu ZS, Li RT, Li XL, Wu W, Jiang XQ, Liu BR. Acs Nano. 2011; 5:2520. [PubMed: 21428432] Hou QP, Chau DYS, Pratoomsoot C, Tighe PJ, Dua HS, Shakesheff KM, Rose FRAJ. J Pharm Sci-Us. 2008; 97:3972.
23. Ferreira LS, Gerecht S, Fuller J, Shieh HF, Vunjak-Novakovic G, Langer R. Biomaterials. 2007; 28:2706. [PubMed: 17346788] Wang X, Wenk E, Zhang X, Meinel L, Vunjak-Novakovic G, Kaplan DL. J Control Release. 2009; 134:81. [PubMed: 19071168]
24. Sharif S, Ohagan DT. Int J Pharm. 1995; 115:259.
25. van de Weert M, Hennink WE, Jiskoot W. Pharm Res. 2000; 17:1159. [PubMed: 11145219]
26. Bilati U, Allemann E, Doelker E. Eur J Pharm Biopharm. 2005; 59:375. [PubMed: 15760718]
27. Yilgor P, Tuzlakoglu K, Reis RL, Hasirci N, Hasirci V. Biomaterials. 2009; 30:3551. [PubMed: 19361857]
28. Kim S, Kang YQ, Krueger CA, Sen ML, Holcomb JB, Chen D, Wenke JC, Yang YZ. Acta Biomater. 2012; 8:1768. [PubMed: 22293583]
29. Patel ZS, Young S, Tabata Y, Jansen JA, Wong MEK, Mikos AG. Bone. 2008; 43:931. [PubMed: 18675385]
30. Richardson TP, Peters MC, Ennett AB, Mooney DJ. Nat Biotechnol. 2001; 19:1029. [PubMed: 11689847]

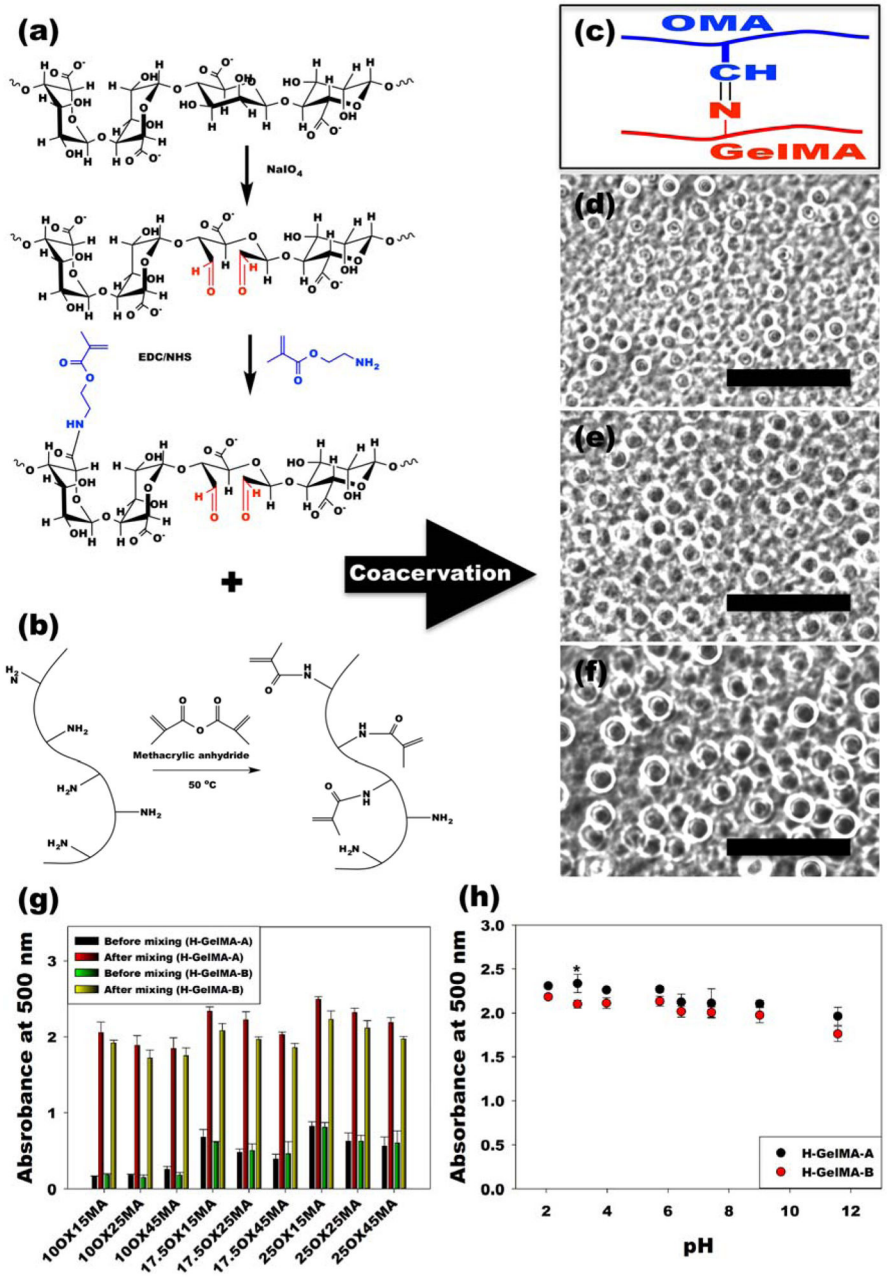

Figure 1. Formation of OMA/GelMA coacervates

(a–b), Schematic illustrations of preparation and chemical structures of **(a)** OMA and **(b)** GelMA. **(c)** Schematic illustration of Schiff base reaction between the aldehyde group of the OMA and amine group of the GelMA. **(d–f),** Representative optical photomicrographs of OMA/GelMA coacervate microdroplets formed by **(d)** 17.5OX15MA and H-GelMA-B, **(e)** 17.5OX25MA and H-GelMA-B, and **(f)** 17.5OX45MA and H-GelMA-B. The scale bars indicate 100 μm. **(g)** Turbidity of OMA/GelMA solutions prepared at pH 7.4 before and after mixing of two solutions by the measurement of the absorbance at 500 nm to evaluate the degrees of complex coacervate formation. **(h)** Turbidity of OMA (25OX45MA)/H-GelMA coacervate as a function of pH. All quantitative data is expressed as mean ±

standard deviation (N=3). Statistical analysis was performed with one-way analysis of variance (ANOVA) with Tukey significant difference post hoc test using Origin software (OriginLab Co). The absorbance of all groups significantly increased after mixing ($p<0.001$). *$p<0.05$ compared with H-GelMA-B at a specific pH.

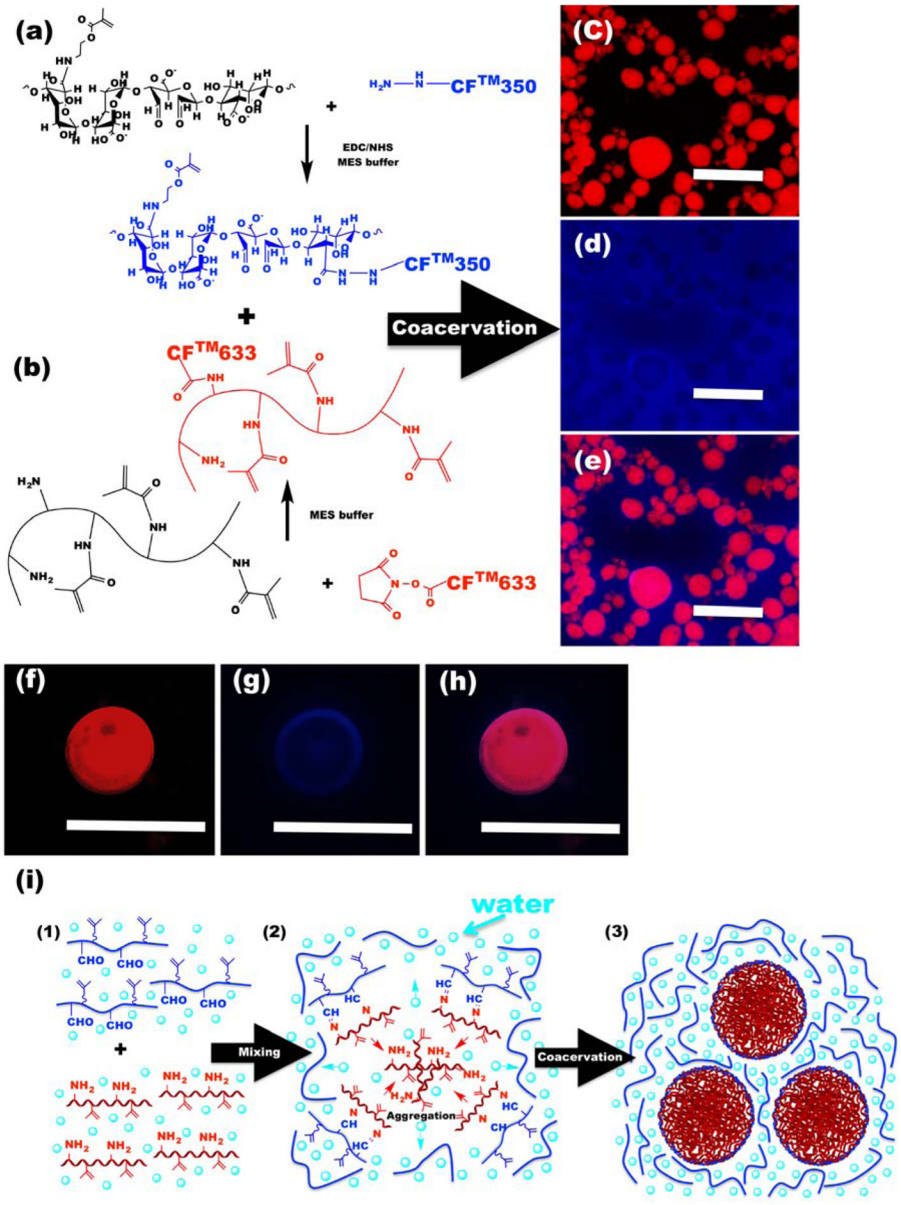

Figure 2. Microstructural characterization of OMA/GelMA coacervates

(a–b), Schematic illustrations for synthesis of fluorescently-labeled **(a)** 17.5OX15MA and **(b)** H-GelMA-A. **(c–e),** Representative fluorescence photomicrographs of OMA/GelMA coacervates. **(c)** Red channel, **(d)** blue channel and **(e)** merged image. **(f–h),** Representative fluorescence photomicrographs of individual OMA/GelMA coacervate microdroplet with high magnification. **(f)** Red channel, **(g)** blue channel and **(h)** merged image. The scale bars indicate 50 μm. **(i)** Schematic representation of the formation of OMA/GelMA coacervate microdroplets.

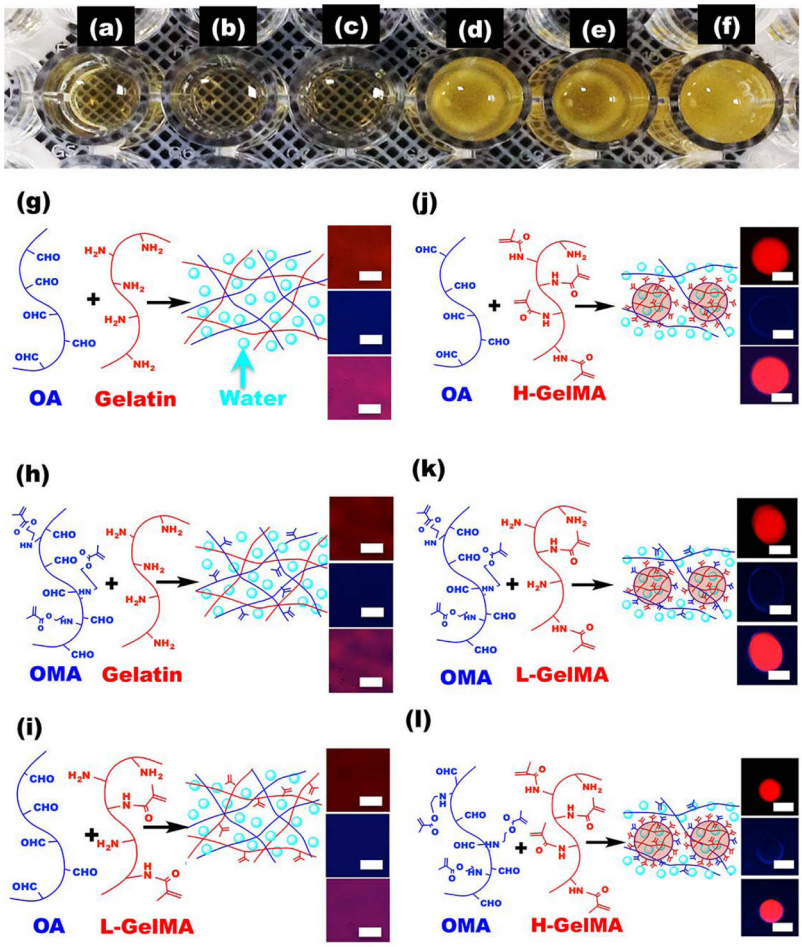

Figure 3. Effect of alginate and gelatin methacrylation on coacervate formation

(a–f), Representative photograph of **(a)** OA/Gelatin, **(b)** OMA/Gelatin, **(c)** OA/L-GelMA, **(d)** OA/H-GelMA, **(e)** OMA/L-GelMA and **(f)** OMA/H-GelMA mixtures in a 96-well plate. **(g–h),** Schematic microstructure and representative fluorescence images [red channel (top), blue channel (middle), and merged image (bottom)] of **(g)** OA/Gelatin, **(h)** OMA/Gelatin, **(i)** OA/L-GelMA, **(j)** OA/H-GelMA, **(k)** OMA/L-GelMA and **(l)** OMA/H-GelMA mixtures. The scale bars indicate 30 μm.

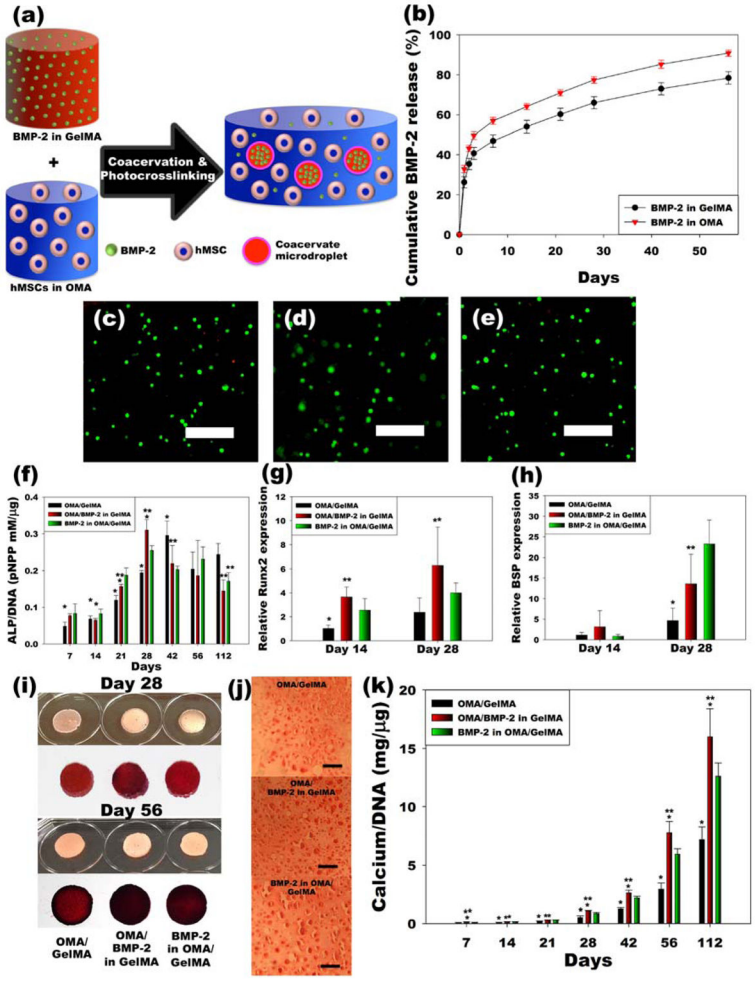

Figure 4. Phothoencapsulation of hMSCs and BMP-2 in OMA/GelMA coacervate hydrogels induces hMSC osteogenesis

(a) Schematic illustration of *in situ* formation of BMP-2-loaded coacervate microdroplets-embedded hydrogel for osteogenic differentiation of photoencapsulated hMSC. **(b)** Release profiles of BMP-2 from photocrosslinked OMA/BMP-2 in GelMA and BMP-2 in OMA/GelMA coacervate microdroplet-laden hydrogels (N=5). **(c–e),** Live/Dead staining of encapsulated hMSCs in photocrosslinked **(c)** OMA/GelMA, **(d)** OMA/BMP-2 in GelMA and **(e)** BMP-2 in OMA/GelMA coacervate microdroplet-laden hydrogels after 28 days culture in osteogenic differentiation media. **(f–h),** Quantification of **(f)** ALP/DNA (N=6), and **(g)** relative Runx2 (N=6) and **(h)** BSP (N=6) gene expression in hMSCs encapsulated within hydrogels. **(i–k),** Mineralization of cell-hydrogel constructs analyzed by **(i and j)** Alizarin red staining and **(j)** quantification of calcium content (N=6) in the constructs. The scale bars indicate 100 μm. All quantitative data is expressed as mean ± standard deviation. Statistical analysis was performed with one-way analysis of variance (ANOVA) with Tukey significant difference post hoc test using Origin software. *p<0.05 compared with BMP-2 in OMA/GelMA group at a specific time point. **p<0.05 compared with OMA/GelMA group at a specific time point.